

Impact of the New England Seamount Chain on Gulf Stream Pathway and Variability

ERIC P. CHASSIGNET¹, XIAOBIAO XU¹, ALEXANDRA BOZEC¹, AND TAKAYA UCHIDA^{1,2}

¹Center for Ocean-Atmospheric Prediction Studies, Florida State University, Tallahassee, Florida

²Université Grenoble Alpes, CNRS, INRAE, IRD, Grenoble INP, Institut des Géosciences de l'Environnement, Grenoble, France

(Manuscript received 17 January 2023, in final form 24 April 2023, accepted 27 April 2023)

ABSTRACT: The potential role of the New England seamount chain (NESC) on the Gulf Stream pathway and variability has been long recognized, and the series of numerical experiments presented in this paper further emphasize the importance of properly resolving the NESC when modeling the Gulf Stream. The NESC has a strong impact on the Gulf Stream pathway and variability, as demonstrated by comparison experiments with and without the NESC. With the NESC removed from the model bathymetry, the Gulf Stream remains a stable coherent jet much farther east than in the experiment with the NESC. The NESC is the leading factor destabilizing the Gulf Stream and, when it is not properly resolved by the model's grid, its impact on the Gulf Stream's pathway and variability is surprisingly large. A high-resolution bathymetry, which better resolves the New England seamounts (i.e., narrower and rising higher in the water column), leads to a tighter Gulf Stream mean path that better agrees with the observed path and a sea surface height variability distribution that is in excellent agreement with the observations.

KEYWORDS: North Atlantic Ocean; Boundary currents; Mesoscale processes; General circulation models; Numerical analysis/modeling; Topographic effects

1. Introduction

In Chassignet and Xu (2017), the authors argued that the next threshold for a significant improvement in western boundary currents representation (i.e., the Gulf Stream in their paper) is an increase in the horizontal resolution from an eddying $1/10^\circ$ to a submesoscale enabled $1/50^\circ$ grid spacing. They showed that, as the resolution is increased from $1/12^\circ$ to $1/50^\circ$ (~ 1.5 km at midlatitudes), the representation of the Gulf Stream eastward penetration and associated recirculating gyres shifts from unrealistic to realistic and that the penetration of eddy kinetic energy (EKE) into the deep ocean is drastically improved and closely resembles the observations. They noted, however, several discrepancies between the high-resolution $1/50^\circ$ numerical simulation and observations. The first was a lack of variability in the modeled sea surface height (SSH) wavenumber spectral slope in the mesoscale range between high/midlatitudes and the equator. Xu et al. (2022) recently demonstrated that tidal forcing needs to be included in the simulation to generate high-frequency steric SSH variability from internal tides and to flatten the spectral slope in the equatorial region as in the observations. Another notable discrepancy was an area of high SSH variability and surface EKE wider than in the observations near the New England seamount chain (NESC). This suggests that interactions with the topography (i.e., the NESC) may be overemphasized in this model configuration (Chassignet and Xu 2021). The goal in Chassignet and Xu (2017) was to perform a convergence study in which most parameters were not changed as the grid

spacing was refined from $1/12^\circ$ to $1/50^\circ$ and the bathymetry used for their $1/50^\circ$ configuration was therefore linearly interpolated from the coarser $1/12^\circ$ topography based on the 2' (i.e., 2 min of lat/lon) Naval Research Laboratory (NRL) digital bathymetry database. The question then arises as to whether the modeled Gulf Stream pathway and variability would be modified if a higher-resolution bathymetry was used.

There is strong evidence that bathymetry affects time-dependent motion throughout the water column [see LaCasce and Groeskamp (2020) for a review] and the potential role of the NESC on the Gulf Stream pathway and variability has been long recognized. In the very first systematic description of the Gulf Stream between Cape Hatteras and the Grand Banks, Fuglister (1963) noted that the Gulf Stream meander pattern exhibits "an abrupt change, near 62°W , from small amplitude to very large amplitude." Indeed, there is substantial evidence from both in situ and satellite observations that the meanders and variability of the Gulf Stream increase significantly near the NESC (e.g., Hansen 1970; Vastano and Warren 1976; Richardson 1981; Cornillon 1986; Auer 1987; Teague and Hallock 1990; Andres 2016; Seidov et al. 2019). Although there are studies on instability-driven eddy generation when the Gulf Stream leaves the shallow continental slope near 68°W (e.g., Savidge and Bane 1999; Kämpf 2005; Schubert et al. 2018), there is, however, surprisingly little in the literature on the mechanisms behind NESC-induced instabilities and the impact of the NESC on the Gulf Stream pathway and variability has never been fully investigated. Adamec (1988) and Ezer (1994) are the only two modeling studies that we are aware of that attempted to quantify its impact using idealized or regional numerical models. Ezer (1994) found that the effects of the NESC on the Gulf Stream included the development of several quasi-stationary, nearly barotropic recirculation cells near the seamounts as well as a shift in the region of large EKE upstream of the NESC. Both studies suggest

 Denotes content that is immediately available upon publication as open access.

Corresponding author: Eric P. Chassignet, echassignet@fsu.edu

DOI: 10.1175/JPO-D-23-0008.1

© 2023 American Meteorological Society. This published article is licensed under the terms of the default AMS reuse license. For information regarding reuse of this content and general copyright information, consult the AMS Copyright Policy (www.ametsoc.org/PUBSReuseLicenses).

Brought to you by FLORIDA STATE UNIVERSITY | Unauthenticated | Downloaded 08/07/23 01:40 PM UTC

TABLE 1. North and equatorial Atlantic model configurations.

1/50° experiment ($\Delta x \sim 1.5$ km)	Bathymetry
NEATL	2' Naval Research Laboratory ($\Delta x \sim 2.5$ km)
NEATL-HB	15-arc-s GEBCO ($\Delta x \sim 300$ m)
NEATL-HB-NoNESC	Same as NEATL-HB, but with the NESC removed

that the NESC should induce a southward deflection, but this is not observed. If anything, the observed Gulf Stream path exhibits a small northward deflection after passing the NESC.

In this paper, we document in detail the impact of the NESC on the Gulf Stream's pathway and variability and emphasize how a proper representation of the fine-scale structure of the NESC is essential in reproducing the observed Gulf Stream variability. The layout is as follows. In section 2, we investigate the sensitivity of the Gulf Stream pathway to the NESC in a series of 1/50° North and equatorial Atlantic realistic simulations. We first confirm that the NESC strongly impacts the Gulf Stream pathway by removing the NESC from the model's bathymetry as in Ezer (1994). We then show that the inclusion of a high-resolution bathymetry, which better resolves the New England seamounts details (i.e., narrower and rising higher in the water column), leads to a tighter Gulf Stream mean path that better agrees with the observed path. The impact of using a fine-resolution bathymetry on the Gulf Stream is most striking on the surface variability where not only is the excess SSH variability near the NESC found in the experiment with coarse bathymetry eliminated, but the shape and distribution of the variability in the experiment with high-resolution bathymetry is now a very close match to the observations. The reason behind this better agreement is that the instability processes induced by the Gulf Stream interacting with the NESC is strongly dependent

upon how well the bathymetry is represented. In section 3, we quantify the importance of properly representing the NESC by performing a series of idealized experiments illustrative of 1) the earlier experiments of Adamec (1988) and Ezer (1994) and 2) of the 1/50° configurations discussed in section 2. The results are summarized and discussed in section 4.

2. Impact of the bathymetry on Gulf Stream pathway and variability in the 1/50° North and equatorial Atlantic simulations

a. Model configuration

The Hybrid Coordinate Ocean Model (HYCOM) configuration used in this paper is identical to that of Chassignet and Xu (2017) and covers the North Atlantic Ocean from 28°S to 80°N (see their Fig. 1). In this paper, we analyze three 1/50° configurations (2.25 km at the equator; 1.5 km in the Gulf Stream region), identical with each other except for the bathymetry (Table 1). The coarse-resolution model topography in the reference North and equatorial Atlantic (hereinafter referred to as NEATL) experiment of Chassignet and Xu (2017) is linearly interpolated from a coarser 1/12° topography based on the 2' NRL digital bathymetry database, which combines the global topography based on satellite altimetry of Smith and Sandwell (1997) with several high-resolution regional databases. The bathymetry for the high-resolution bathymetry experiment NEATL-HB is derived from the latest 15-arc-s GEBCO bathymetry (https://www.gebcoc.net/data_and_products/gridded_bathymetry_data/) and therefore contains topographic features that have significantly higher resolution (Figs. 1 and 2). The bathymetry in NEATL-HB-NoNESC is identical to that of NEATL-HB, except that the NESC was removed (see Fig. 2 for details). To remove a seamount, we first identify the deepest closed contour of the seamounts and define the area shallower than this contour as the seamount. For the seamounts that sit over the abyssal plain, we simply replace the seamount

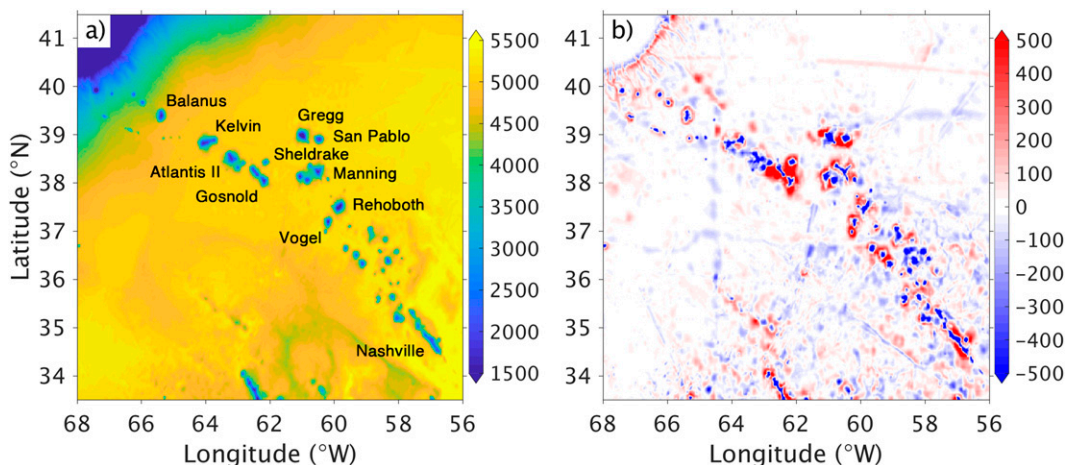


FIG. 1. (a) NEATL-HB bathymetry (m) with the names of the major seamounts (Houghton et al. 1977); (b) difference in bathymetry (m) between NEATL-HB and NEATL, with the bluer color indicating a shallower depth in NEATL-HB and vice versa.

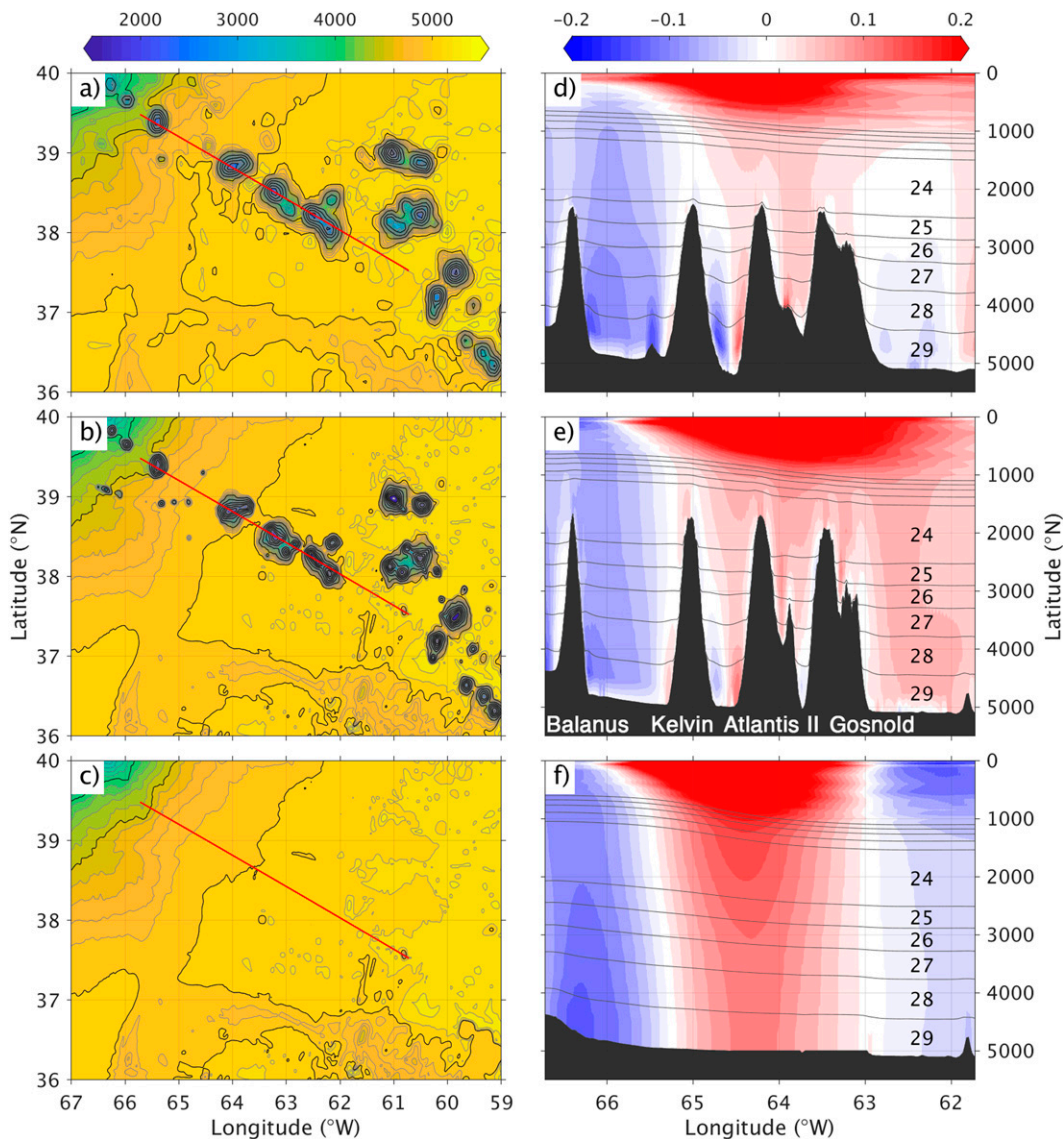


FIG. 2. (a)–(c) Zoomed bathymetry (m) in the NES region and (d)–(f) distribution of the model layer interfaces and the Gulf Stream zonal velocities (m s^{-1}) along the red line in (a)–(c) that transects the four key New England seamounts in the Gulf Stream pathway (Balanus, Kelvin, Atlantic II, and Gosnold) in three simulations: (top) NEATL, (middle) NEATL-HB, and (bottom) NEATL-HB-NoNES. The black and gray depth contours in (a)–(c) are in 500- and 100-meter intervals, respectively. The numbers 24–29 in (d)–(f) are model layer indices (interfaces for the model layers 1–19 are not plotted).

bathymetry with the constant closed contour depth. For the seamounts that sit on the continental slope (15 of them including Kelvin), we replace the seamount bathymetry with the interpolated depth calculated from the background slope without the seamounts.

In the vertical direction, the simulation contains 32 hybrid layers with density referenced to 2000 m (σ_2) [see Chassignet and Xu (2017) for details]. The vertical coordinate in HYCOM (Bleck 2002) is isopycnal in the stratified open ocean and makes a dynamically smooth and time-dependent transition to terrain-following in shallow coastal regions and to fixed pressure levels in the surface mixed layer and/or unstratified seas (Chassignet

et al. 2003, 2006). No inflow or outflow is prescribed at the northern and southern boundaries. Within a buffer zone of about 3° from the northern and southern boundaries, the 3D model temperature, salinity, and depth of isopycnal interface are restored to the monthly Generalized Digital Environmental Model (GDEM) (Teague et al. 1990; Carnes 2009) climatology with an e -folding time of 5–60 days that increases with distance from the boundary. The reference configuration NEATL is initialized using potential temperature and salinity from the GDEM climatology and spun up from rest for 20 years using climatological atmospheric forcing from the ECMWF reanalysis ERA40 (Uppala et al. 2005) with 3-hourly wind anomalies from

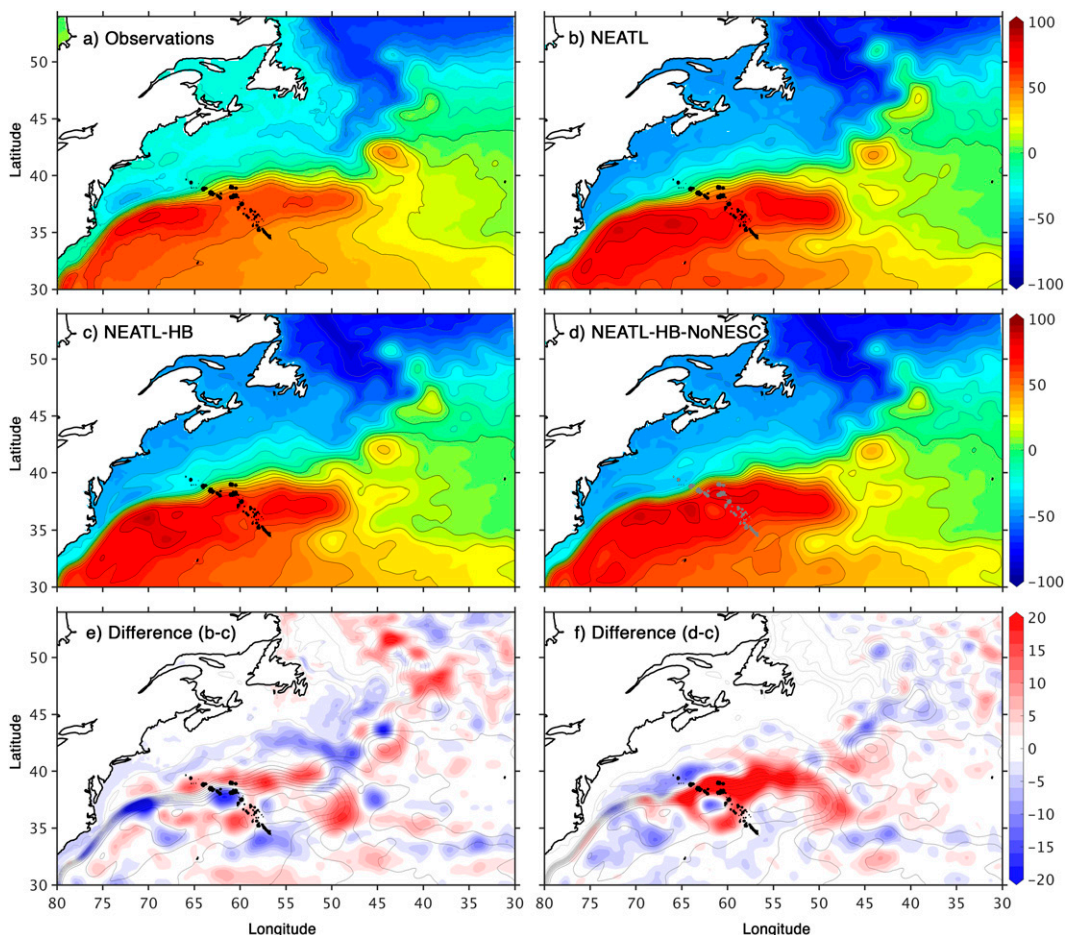


FIG. 3. Mean sea surface height (cm) in the Gulf Stream region based on (a) observations [1993–2018; CNES-CLS18 from Mulet et al. (2021)], (b) NEATL, (c) NEATL-HB, and (d) NEATL-HB-NoNESCS (years 16–20). Also shown are the differences between NEATL-HB and (e) NEATL or (f) NEATL-HB-NoNESCS. Although NEATL-HB-NoNESCS does not have the seamount chain, the NESCS is also shown in (d) (in gray instead of black) for geographical reference.

the Fleet Numerical Meteorology and Oceanography Center 3-hourly Navy Operational Global Atmospheric Prediction System (NOGAPS) for 2003. The year 2003 is considered a neutral year over the 1993–present timeframe in terms of long-term atmospheric patterns, such as the North Atlantic Oscillation. Both NEATL-HB and NEATL-HB-NoNESCS were initialized from the end of year 15 of NEATL and integrated for 5 years. The basin kinetic energy adjusts quickly in less than a year (Chassignet and Xu 2017) and there are no substantial differences in the yearly means. The reader is referred to Chassignet and Xu (2017) for details on the parameterizations used in the model.

b. Impact of the New England seamount chain on the Gulf Stream pathway

As stated in the introduction, observations indicate that the NESCS plays a role in shaping the Gulf Stream pathway and variability (Fuglister 1963; Cornillon 1986; Auer 1987; Teague and Hallock 1990; Andres 2016; Silver et al. 2021). Ezer (1994), using a coarse-resolution regional model, found that the effects of the NESCS on the Gulf Stream included the

development of several quasi-stationary, nearly barotropic recirculation cells on both sides of the Gulf Stream as well as a southward deflection as it passes across the NESCS. The latter is, however, not observed, nor is it present in our $1/50^\circ$ simulations (Fig. 3). To document how the NESCS affects the Gulf Stream dynamics, we examine the impact of 1) including fine-resolution details of the NESCS bathymetry (NEATL-HB vs NEATL) and, 2) as in Ezer (1994), removing the NESCS (NEATL-HB-NoNESCS vs NEATL-HB).

The 5-yr mean SSH for NEATL (coarse bathymetry) and NEATL-HB (fine bathymetry) are shown in Fig. 3 together with the latest observational estimate (Mulet et al. 2021). Overall, both (Figs. 3b,c) agree well with the observed mean (Fig. 3a), but there is a significant difference in the Gulf Stream mean pathway between the two simulations when the Gulf Stream crosses over the NESCS. In the fine bathymetry experiment NEATL-HB, the SSH contours are much closer to each other, and the pathway is much tighter than in the reference experiment NEATL with coarse $1/12^\circ$ bathymetry and is in better agreement with the observations (Fig. 3a) with a

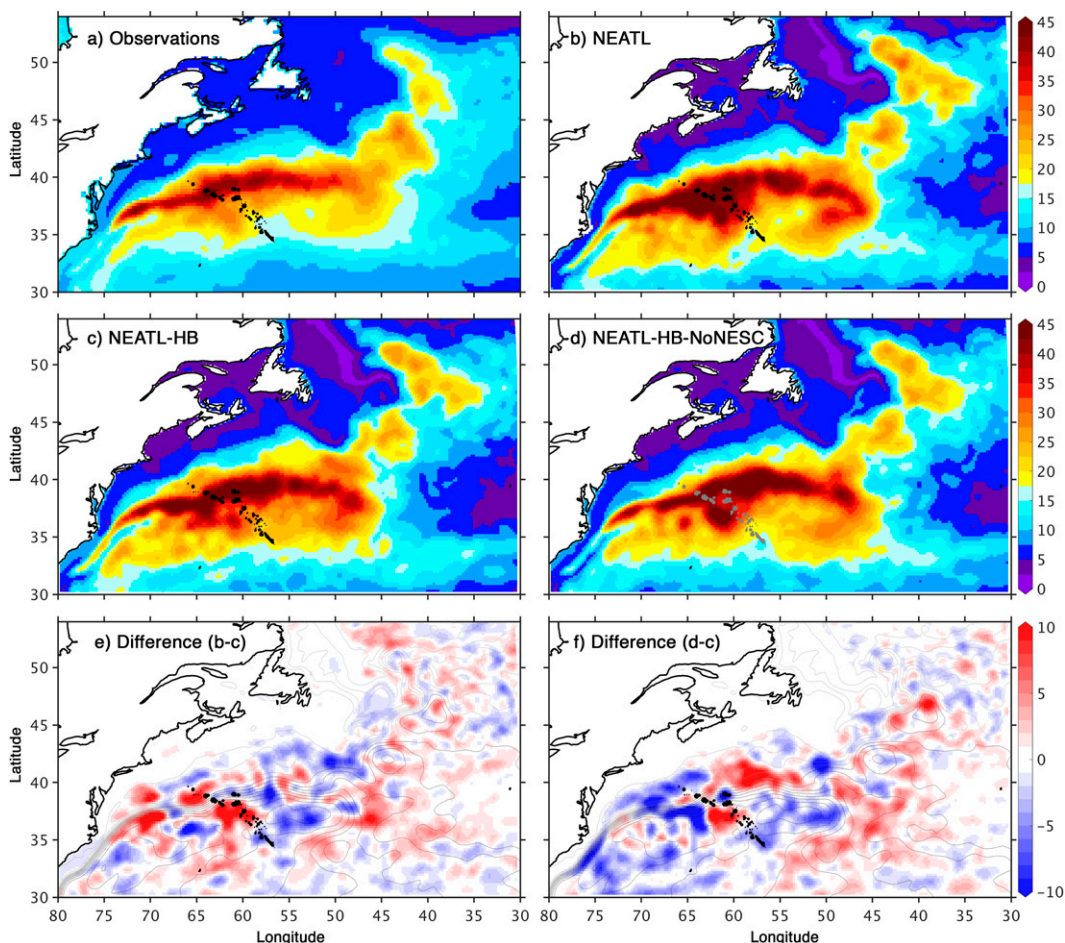


FIG. 4. As in Fig. 3, but for sea surface height variability (cm); the observations are from CMEMS (<https://marine.copernicus.eu>), and the model outputs were filtered to be representative of the CMEMS $1/4^\circ$ gridded outputs by applying a 150-km bandpass filter and averaging the outputs over 10 days on the CMEMS grid [see Chassignet and Xu (2017) for a discussion].

more realistic northward deflection of the Gulf Stream near the NES. The difference in bathymetry between the two experiments is shown in Fig. 1b for the NES region. Away from the seamounts, it is quite small, less than 50 m in most areas. There are, however, two major differences in the representation of the NES in these two experiments (Fig. 2). The first one is in the height of the seamounts. The bathymetry cross sections along the seamount chain (Figs. 2d,e) show that the higher-resolution bathymetry better resolves the New England seamounts and that they rise approximately 500 m higher in the water column and are closer to the base of the permanent thermocline, which is 1000–1500 m according to Meinen and Luther (2016). The second difference is in how the gaps between the seamounts that are located on the southern part of the Gulf Stream are represented, especially the narrow gap between Atlantis II and Gosnold (Figs. 1 and 2). These higher and better-defined topographic features have a significant impact on the Gulf Stream because they not only impact its pathway, but also significantly reduces the instability

processes induced by the Gulf Stream interacting with the NES (see section 2d). This reduced variability leads to a tighter Gulf Stream mean path that better agrees with the observed path (Fig. 3) and a sea surface height variability that is in excellent agreement with the observations (Fig. 4).

Without the NES as in NEATL-HB-NoNES, we find the mean Gulf Stream SSH contours are much closer to each other (Fig. 3d) than in both NEATL and NEATL-HB (Figs. 3b,c), indicative of a more coherent and tighter jet with less variability east of 70°W (Fig. 4). This is quantified in Fig. 5, which displays the north and south walls of the Gulf Stream as a function of longitude for all experiments from which one can infer its width (see Fig. 2 for details). The first thing to note is how narrow the Gulf Stream is when the NES is removed (dark blue contours). Second is how the path of the Gulf Stream's north wall differs between the coarse and fine bathymetry experiments (NEATL and NEATL-HB). In the coarse bathymetry NEATL experiment, the Gulf Stream (light blue contours) widens significantly

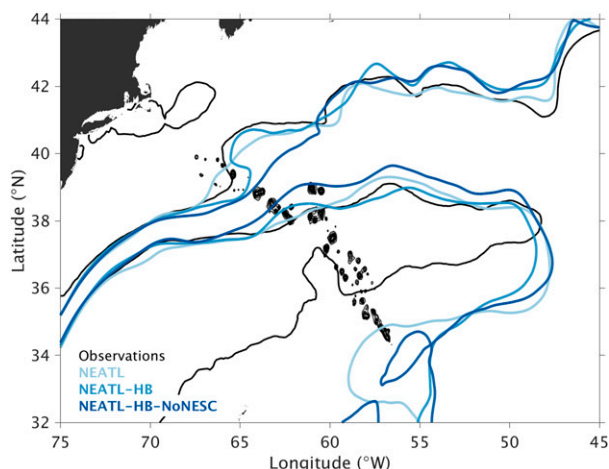


FIG. 5. Time-averaged SSH contours indicating the location for the northern (-25 cm) and southern (50 cm) edge of the Gulf Stream in the northwestern North Atlantic for the three $1/50^\circ$ simulations (NEATL, NEATL-HB, and NEATL-HB-NoNESC). The black contours are the corresponding SSH contours for the observed climatology CNES-CLS18. The location of NESC is indicated by a series of small, closed contours between 68° and 57° W (based on the bathymetry difference between NEATL-HB and NEATL-HB-NoNESC).

before reaching the NESC and shows almost no northward deflection. On the other hand, in the fine bathymetry NEATL-HB experiment, the Gulf Stream's path (blue contours) is close to the observed path (black contours) with no upstream widening and a northward deflection and widening right after going over the NESC. These three experiments clearly demonstrate that the NESC plays a significant role in the Gulf Stream path with increased variability east of 65° W (the longitude at which the Gulf Stream crosses the NESC), as surmised by many authors (e.g., Thompson and Schmitz 1989; Teague and Hallock 1990; Ezer 1994; Hurlburt and Hogan 2000; Gangopadhyay et al. 2016).

c. Impact of the New England seamount chain on the Gulf Stream variability

The impact of the fine-resolution bathymetry and a better NESC representation on the Gulf Stream is even more striking in the plots of SSH variability (Fig. 4) than in the mean SSH plots (Fig. 3). Not only is the excess SSH variability near the NESC found in the experiment with coarse bathymetry (NEATL) eliminated, but the shape and distribution of the variability found in the experiment with high-resolution bathymetry (NEATL-HB) is now a very close match to the observations. This includes a deflection of the variability to the north near 65° W when the Gulf Stream passes over the NESC that is not visible in NEATL.

The widening of the SSH mean contours for the NEATL and NEATL-HB experiments is consistent with the distribution of SSH variability, as shown in Fig. 6 (zoomed SSH variability on the NESC with overlaid bathymetry). Significantly more Gulf Stream variability can be seen upstream of the

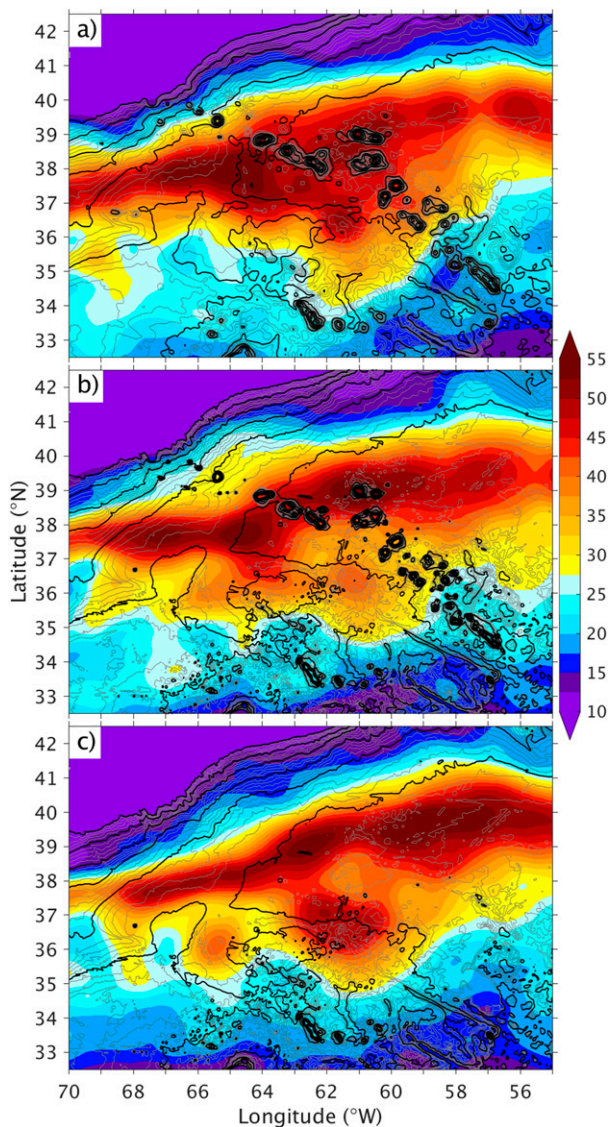


FIG. 6. Sea surface height variability (cm) superimposed on the bathymetry for (a) NEATL, (b) NEATL-HB, and (c) NEATL-HB-NoNESC (years 16–20).

NESC in the coarse bathymetry experiment NEATL than in the fine bathymetry experiment NEATL-HB. This variability leads to a wider mean Gulf Stream (light blue contours in Fig. 5). Variability upstream of the seamounts was also obtained by Ezer (1994) in his regional model, which uses a coarser bathymetry than NEATL. The SSH variability is more confined along the Gulf Stream path in NEATL-HB (Fig. 6) and the widening of the path occurs downstream of the NESC, as for the observations (Fig. 5). In the absence of the NESC, the distribution of the SSH variability is very narrow and the widening of the Gulf Stream path occurs much farther downstream of the NESC's longitude.

The surface signature in SSH variability (Fig. 6) is a direct consequence of the Gulf Stream barotropic velocity component

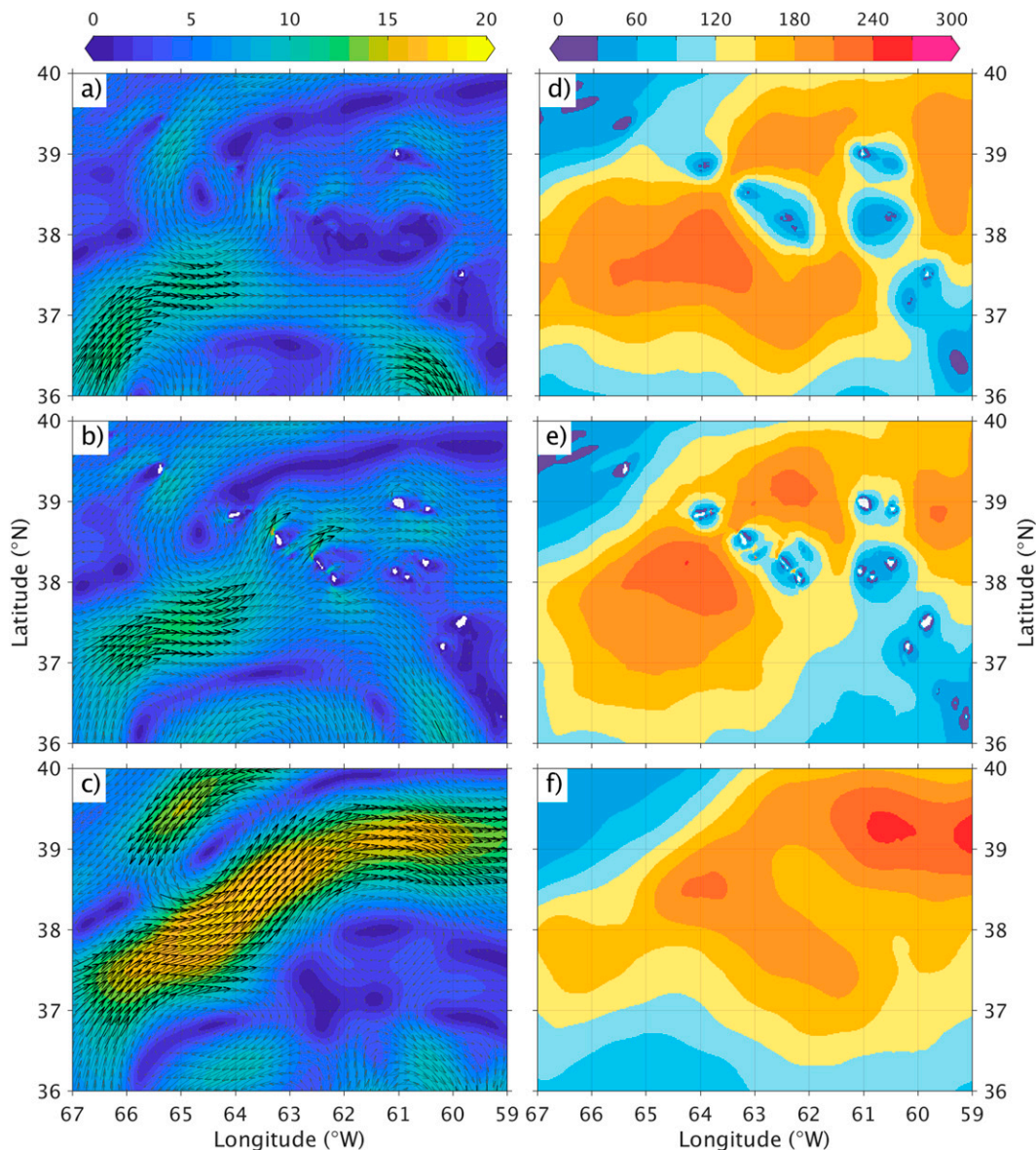


FIG. 7. Time mean (a)–(c) velocity (cm s^{-1}) and (d)–(f) EKE ($\text{cm}^2 \text{s}^{-2}$) in model layer 25 (2300–2500 m) in three experiments: (top) NEATL, (middle) NEATL-HB, and (bottom) NEATL-HB-NoNESC. This layer is located well below the main thermocline across the Gulf Stream (see Figs. 2d–f for the vertical distribution of layer interfaces) and starts to interact with the NESC directly. In (a)–(c), every 1 of 8 grid points in the zonal and meridional directions are plotted. The color shading is the magnitude of the current; the black arrows indicate mean velocity exceeding 10 cm s^{-1} .

interacting with the NESC topography. The vertical coherence of the flow (Fig. 2) is illustrated by comparing Figs. 6–8 that display SSH variability, mean velocities and EKE for model layer 25 and the model bottom layer, respectively. Layer 25 (see Fig. 2) is located near the middle of the North Atlantic Deep Water and is close to the seamounts' tops. From Fig. 2, we can see that for, in the depth range of 4500–5000 m, the Atlantis II and Gosnold seamounts are essentially “merged” in NEATL forming a ridge that is at least 500 m above the abyssal plane ($\sim 5000 \text{ m}$). The end result is that the interior and deep flows

(Figs. 7a,b and 8a,b) are mostly blocked by the seamounts and are steered in large part to the north (through the gap between Kelvin and Atlantis II), but also to the south (through the gap between the Manning and Rehoboth seamounts). There is a correspondingly much larger extent of EKE upstream of the NESC in layer 25 and in the bottom layer in NEATL than in NEATL-HB (Figs. 7c,d and 8c,d). In NEATL-HB, the interior and deep Gulf Stream flows are allowed to pass through the narrow gap between Atlantis II and Gosnold as well as through the gap between Gosnold and Manning, leading to a narrower

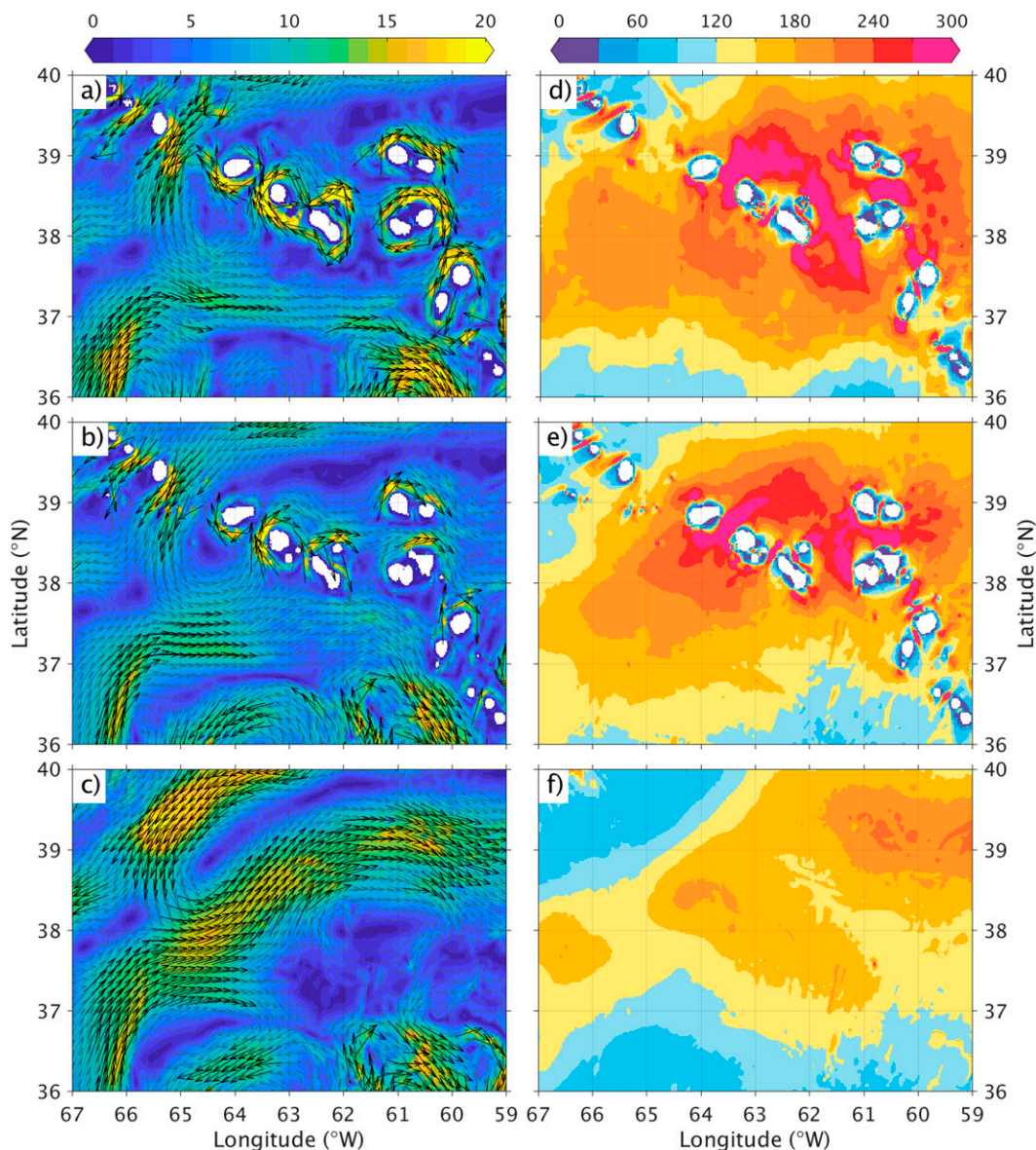


FIG. 8. As in Fig. 7, but for model layer 29 near the bottom (see Figs. 2d–f for the vertical distribution of this layer). Note the significantly wider area of high EKE along the NESc in NEATL and much less EKE in the NEATL-HB-NoNESc.

Gulf Stream when compared with NEATL. When the NESc is removed as in NEATL-HB-NoNESc, there are no obstacles for the deep Gulf Stream, and the Gulf Stream is not only narrower than in NEATL and NEATL-HB, but it is also significantly stronger. The bottom-layer EKE magnitude is also substantially lower in NEATL-HB-NoNESc than in both experiments that include the New England seamount chain (Fig. 8). As stated by Mertz and Wright (1992), the combination of baroclinicity and bottom topography can give rise to a driving force for the depth-averaged flow. A proper representation of the so-called joint effect of baroclinicity and relief (JEBAR) has been shown by Holland and Hirschman (1972) in early modeling studies to lead to a more realistic Gulf Stream

transport and, more recently, to strongly impact the North Atlantic vorticity balance (Schoonover et al. 2016).

d. Linear stability analysis

A wider mean pathway together with enhanced downstream EKE is indicative of enhanced instabilities near the NESc in NEATL. In this section, we examine how the presence of the NESc affects the linear stability of the flow. We do so by diagnosing the baroclinic instability growth rates linearized about a background flow. Namely, we solve for the linear quasigeostrophic (QG) eigenvalue problem under a β -plane approximation by prescribing the local profile of velocity \mathbf{U} and stratification N^2 at each point as the background

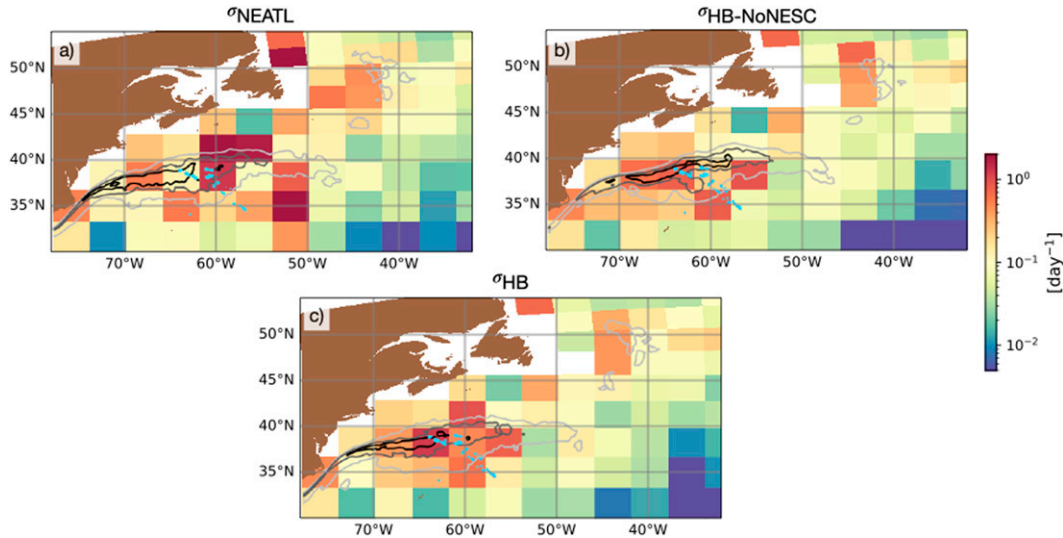


FIG. 9. Baroclinic instability growth rates for the runs (a) NEATL, (b) NEATL-HB-NoNESC, and (c) NEATL-HB plotted for regions where the bathymetry is deeper than 500 m. The surface EKE is shown in contours, with gray shading for the values of 0.2, 0.35, and 0.5 $\text{m}^2 \text{s}^{-2}$. NESC is marked as the cyan dots. Although NEATL-HB-NoNESC does not have the seamount chain, it is shown in (b) for geographical reference.

flow (Smith 2007; Uchida et al. 2017; Yankovsky et al. 2022) and by fitting a plane-wave solution $\psi = \text{Re}[\Phi(z)e^{i(kx+ly-\omega t)}]$ to the potential vorticity equation

$$\frac{\partial q}{\partial t} + \mathbf{U} \cdot \nabla q + \mathbf{u}^{\text{qs}} \cdot \nabla Q = 0,$$

where $\text{Re}[\cdot]$ is the real part of \cdot and the QG potential vorticity q and velocity \mathbf{u}^{qs} are related to the streamfunction ψ as

$$q = \nabla^2 \psi + \frac{\partial}{\partial z} \left(\frac{f^2}{N^2} \frac{\partial \psi}{\partial z} \right)$$

and $\mathbf{u}^{\text{qs}} = \nabla \times \psi$, respectively. The background potential vorticity is $Q = \beta y$, and the background velocity is \mathbf{U} (defined below). The boundary condition is

$$\frac{\partial b}{\partial t} + \mathbf{U} \cdot \nabla b + \mathbf{u}^{\text{qs}} \cdot \nabla (B + N^2 \eta) = 0,$$

where $b = f(\partial \psi / \partial z)$ and $B = \int N^2 dz$ are the perturbation and background buoyancy, respectively, and η represents the vortex-tube stretching due to topographic slope and sea surface height. Imaginary parts in ω correspond to infinite growth and thus to the growth rates (Vallis 2017). Although QG conditions are not fully met in the separated Gulf Stream region (Chassignet and Xu 2017; Jamet et al. 2021), the growth rates provide a qualitative description of baroclinicity.

The background flow here is defined by a 5-yr temporal averaging and 200×200 gridpoint boxcar spatial coarse graining in the horizontal dimensions, which nominally corresponds to $4^\circ \times 4^\circ$ in latitude and longitude. The N^2 was diagnosed from the 5-yr averaged potential temperature and practical salinity outputs at $1/50^\circ$ using the GSW Python package prior to coarse graining (<https://teos-10.github.io/GSW-Python/>; McDougall

and Baker 2011). To take into consideration the finite-volume nature of HYCOM, momentum was weighted by the cell face area and tracers by the cell volume in the process of coarse graining; the background flow can be considered to be thickness-weighted averaged in the spatial sense [e.g., $\mathbf{U} = \overline{(\mathbf{u}h^p)} / \overline{h^p}$, where \mathbf{u} is the 5-yr averaged horizontal velocity outputs at $1/50^\circ$, h^p is the 5-yr averaged isopycnal layer thickness at $1/50^\circ$, and $\overline{(\cdot)}$ is the spatial coarse graining operator; Young 2012; Li et al. 2019]. The time-space-filtered background flow and stratification along isopycnals were then vertically remapped onto a monotonic geopotential coordinate with 75 layers using the XGCM Python package (<https://xgcm.readthedocs.io/en/latest/>; Abernathy et al. 2023) in order to reduce the discretization errors in solving for the eigenvalue problem. Negative stratification values ($N^2 < 0$) were vertically linearly interpolated over to maintain a stable background. We prescribed a rigid lid and flat bottom (i.e., $\eta = 0$) since the coarse graining conflates various topographic and sea surface conditions. As the background flow is taken via a time mean, the background flow includes the effect of standing eddies as a result of the presence of NESC or the lack thereof and the instabilities should reflect this.

Figure 9 exhibits the maximum growth rates for the region around the separated Gulf Stream for all three cases (σ_{NEATL} , σ_{HB} , and $\sigma_{\text{HB-NoNESC}}$ corresponding to NEATL, NEATL-HB, and NEATL-NB-NoNESC, respectively, where $\sigma = \text{Im}[\omega]$ is the imaginary part of ω). Consistent to what we would expect from the stability in Gulf Stream paths (Fig. 5) and also from the idealized experiments described in the following section, the growth rates are higher in the northeastern wake of the seamount chain in NEATL and NEATL-HB than in NEATL-HB-NoNESC, which has no seamount chain. In other words, the presence of the NESC decreases the stability of the flow downstream of the

TABLE 2. First set of idealized jet experiments with a grid spacing of 10 km.

Expt	Half-width W (km) of seamount	Height H (m) of seamount
C1	150	500
C2	150	3000
C3	40	500
C4	40	3000
C5	20	500
C6	20	3000

seamount chain in the path of the separated Gulf Stream. Furthermore, the flow is more unstable in NEATL with the coarse bathymetry (dark red patches) than in NEATL-HB with the fine bathymetry (orange patches), in agreement with the greater variability downstream of the NES in NEATL.

3. Impact of the bathymetry on a midlatitude jet in idealized experiments

When comparing the midlatitude jet path with and without the NES, we do not find that the NES induces a southward deflection as in Adamec (1988) and Ezer (1994) and as one may expect from potential vorticity conservation (Holton and Hakim 2013). If anything, the observations seem to indicate that the NES induces a small northward deflection (Figs. 3–5). One of the main differences between these two earlier studies and the experiments presented here is the much coarser horizontal resolution in Adamec (1988) and Ezer (1994) (~15–20 km versus 1.5 km). The larger grid spacing implies a coarser representation of the NES and therefore what we surmise is a stronger interaction with the surface jet, i.e., the Gulf Stream. This hypothesis motivates us to quantitatively document the impact of properly resolving the seamounts' shapes and heights on the upper circulation (pathway and instabilities) and explain the differences between our results and those of Ezer (1994) as well as the differences between NEATL and NEATL-HB. In this section, we perform a series of zonal jet idealized experiments with varying horizontal grid spacing and varying seamounts' widths and heights.

The configuration of the HYCOM idealized model used in this section is a $5000 \times 1000 \text{ km}^2$ two-layer channel on a β -plane representative of the Gulf Stream region. The two layers have resting thicknesses of 1000 and 4000 m, respectively, with $g' = 0.016 \text{ m s}^{-2}$. The imposed boundary conditions are designed to drive an eastward flowing jet representative of the Gulf Stream. In the western part of the domain, the inflow open boundary conditions are prescribed over the first 500 km

and consist of a zonal jet corresponding to an interface displacement of 800 m over a 100-km width and an average core velocity of 0.8 m s^{-1} in the upper 1000-m layer. The outflow boundary conditions in the eastern part of the domain are identical to the inflow, except they are prescribed over 100 km. Interface heights are weakly restored (20 days) at the northern and southern boundaries over 100 km to maintain the cross-isopycnal slope. This configuration is conceptually very similar to the one used by Barthel et al. (2017) to investigate jet-topography interactions in the Southern Ocean. All simulations are run for three years, and we look at the time mean of the last two years. Two sets of experiments are performed (Tables 2 and 3). The first set uses a coarse horizontal grid $\Delta x = 10 \text{ km}$ to match the 10–20-km grid spacing used in the numerical studies of Verron et al. (1987), Adamec (1988), and Ezer (1994). The second set uses a fine horizontal grid $\Delta x = 2 \text{ km}$ to investigate the impact of the bathymetry difference between NEATL and NEATL-HB.

Adamec (1988) investigated the impact of the NES in an idealized quasigeostrophic two-gyre configuration and found that the prescribed chain of seamounts deflected the eastward jet southward. In that case, the chain of seamounts induced a flow pattern very similar to the one generated by a ridge, as in Verron et al. (1987). Ezer (1994) used a regional model of the northwestern Atlantic ($80^\circ\text{--}50^\circ\text{W}$, $30^\circ\text{--}47^\circ\text{N}$) to compare a simulation with full bottom topography with one without the NES (but with all other topographic features remaining the same). As in the idealized studies of Verron et al. (1987) and Adamec (1988), the effect of the NES in Ezer (1994) is a southward deflection of the modeled Gulf Stream. In summary, a common finding of all these early idealized and regional numerical studies is that the NES topography deflects the eastward jet southward. While such a displacement is consistent with potential vorticity conservation (Holton and Hakim 2013), the observed Gulf Stream path does not exhibit a southward deflection; on the contrary, it could be argued that there is actually a small northward deflection (Figs. 3a and 5) at the NES. We therefore surmise that the modeled NES topographies prescribed by Adamec (1988) and Ezer (1994) are coarser and larger than the real topography because of the inability of the horizontal model grid (10–20 km) to properly resolve a 30-km-wide seamount (Huppert and Bryan 1976). This consequently has a strong impact on the upper-layer midlatitude jet representation. In Ezer (1994), not only was the bathymetry coarse to begin with when generated on a 10–17-km grid, additional smoothing was required to minimize pressure gradient errors in the Princeton Ocean Model (Mellor et al. 1994). From Fig. 1 of Ezer (1994), we estimate that the NES is

TABLE 3. Second set of idealized jet experiments with a grid spacing of 2 km.

Expt	Seamount separation Δ (km)	Half-width W (km) of seamounts	Height H (m) of seamounts
F1	50	12	2500
F2	50	6	3000
F3	100	12	2500
F4	100	6	3000

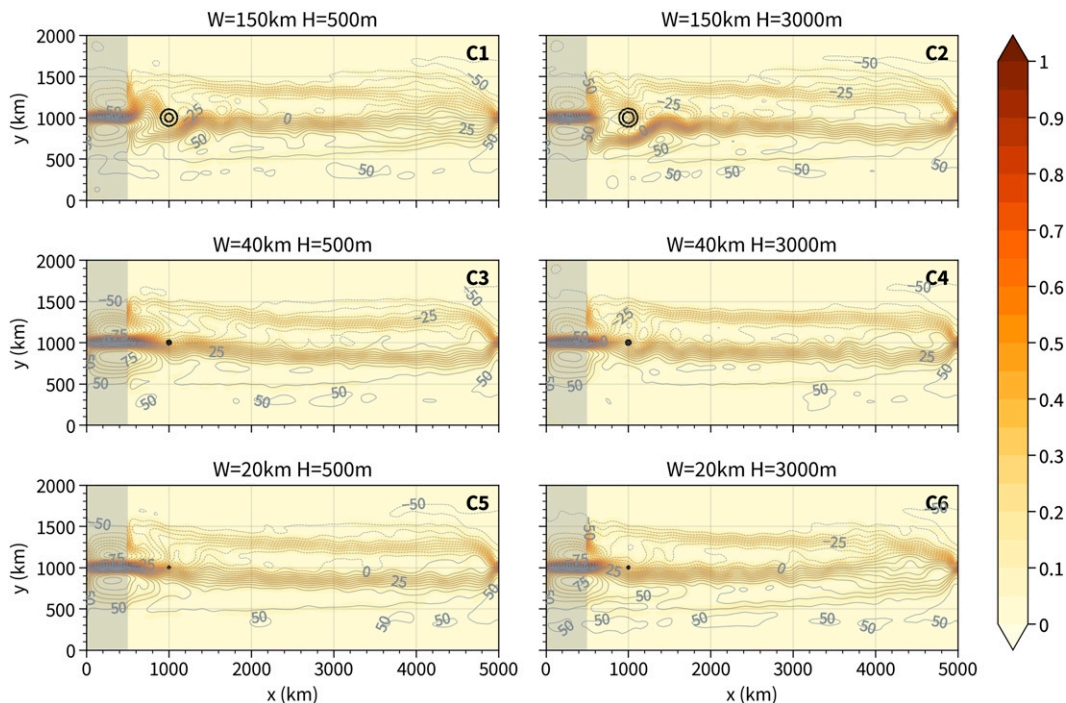


FIG. 10. Two-year mean SSH (cm) for the coarse-resolution experiments C1–C6 (see Table 2) superimposed on the upper-layer velocity (m s^{-1}). The seamount (dark-brown contours) is positioned 500 km downstream of the prescribed open boundary relaxation area (shaded in gray).

approximately 300 km wide with little separation between the seamounts and 1000 m high. To quantify the impact of the seamounts' size on the Gulf Stream, we perform six idealized experiments with a Gaussian seamount

$$h = He^{-\frac{(x-x_0)^2 + (y-y_0)^2}{2W^2}}$$

of half-width W varying from 150 [to mimic the NESC topography of Ezer (1994)] to 20 km with maximum heights H of either 500 or 3000 m (Table 2). These two heights were chosen to bracket the seamounts' height of Ezer (1994) and for comparison with the fine-mesh experiments (Table 3). Not surprisingly, the larger and taller the seamount is, the larger the impact is on the jet's pathway as shown in Fig. 10 (2-yr mean SSH and upper-layer velocity).

With a seamount approximately 300 km wide (experiments C1 and C2), the upper jet exhibits a large meander upstream of the seamount independently of its height (Fig. 10). This is reminiscent of the large southward deflection observed by Adamec (1988) and Ezer (1994). Ezer (1994) stated that “the models tend to overreact to this topographic effect” and we argue here that it is because of the inability of the models to properly resolve the NESC with a 10–20-km grid spacing. It can be shown that the impact on the upper-layer jet is significantly reduced when much narrower seamounts are prescribed (Fig. 10). When the width is reduced to 80 km, there is a much smaller southward deflection and a downstream standing wave. The latter is more pronounced when the seamount height is 3000 m instead of 500 m. The surface signature becomes even smaller with a seamount width of 40 km

(Fig. 10). For reference, we estimate from Fig. 2e that the half-width of the observed NESC seamounts is on the order of 5–10 km [similar to estimates by Vastano and Warren (1976) and Huppert and Bryan (1976)].

This first series of idealized experiments (C1–C6) documents the impact of the seamount size on configurations that use coarse horizontal resolution and smoothed bathymetry, such as Ezer (1994). The second series of idealized experiments (F1–F4) aims at explaining the differences in SSH variability around the NESC observed between NEATL and NEATL-HB. The configuration is identical to that of the coarse experiments (C1–C6), except for the grid spacing (2 km instead of 10 km) and the bathymetry (Table 3). In this second series of experiments, we investigate the impact of two seamounts separated by a distance Δ (Table 3 and Fig. 11) on the surface jet. The goal is to quantify how significant the change of bathymetry of the seamounts Atlantic II and Gosnold (Figs. 2d,f) is on the Gulf Stream pathway and variability between NEATL and NEATL-HB. In NEATL, Atlantic II and Gosnold overlap at their bases with a maximum height of ~ 2500 m (Fig. 2d). In NEATL-HB, Atlantic II and Gosnold are significantly narrower than in NEATL and are well separated from each other with a maximum height of ~ 3000 m (Figs. 1 and 2e).

Not surprisingly, the wider the seamounts are and the closer they are to each other, the stronger the impact is on the surface jet. For a 24-km width and a separation of 50 km, the surface jet develops a standing wave downstream (experiment F1; Fig. 12). On the other side of the spectrum, for a 12-km width and a seamount separation of 100 km, the impact on the

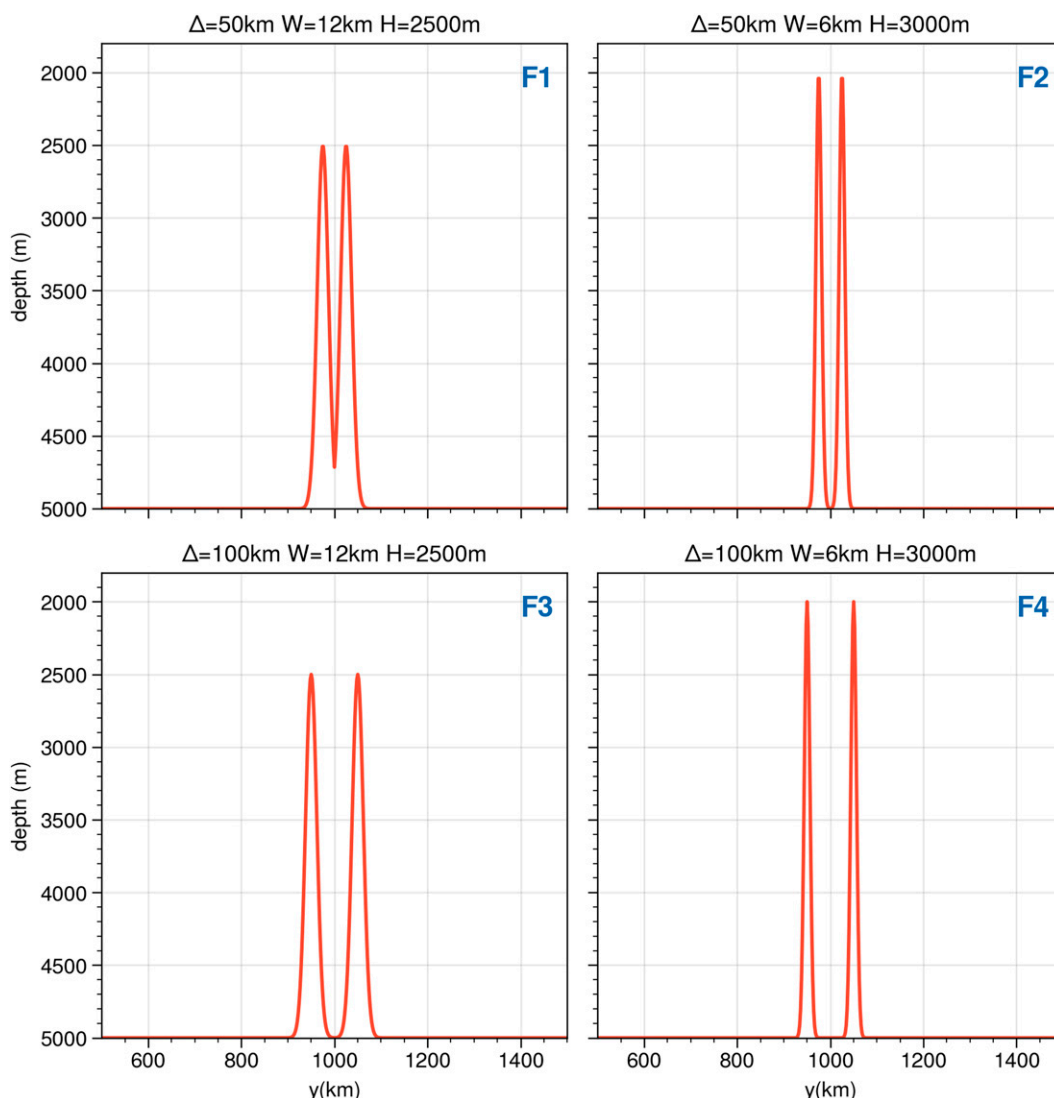


FIG. 11. The dual-seamounts bathymetry used in experiments F1–F4 separated by either (top) 50 or (bottom) 100 km and with heights of either (left) 2500 or (right) 3000 m (Table 3).

surface jet is very small (experiment F4; Fig. 12). For the other combinations (experiments F2 and F3; Fig. 12), the surface signature is in between F1 and F4. The question then arises as to what extent the different seamounts' shapes and separation distances may also affect the surface EKE. In other words, do we see a reduction in EKE with taller and thinner seamounts as implied by the NEATL/NEATL-HB comparison? Figure 13 displays the upper-layer kinetic energy for the four experiments F1–F4, and the meridional extent of the kinetic energy is indeed smaller in experiments F3 and F4 with thinner seamounts and smallest when the seamounts are well separated as seen for F4. The reduction in the spread of EKE as the bathymetry is refined (narrower and taller seamounts) from F1 to F4 is reminiscent of the narrower and more confined EKE/SSH variability found in NEATL-HB, therefore confirming that the change in Gulf Stream pathway and variability

between NEATL and NEATL-HB is a consequence of the better resolved NESC grid spacing in the latter.

The smaller EKE footprint in experiment F4 and, to a lesser degree, in experiment F3, suggest that the instability process is somewhat reduced when seamounts are thinner. To test that hypothesis, experiments F1–F4 are repeated with cyclic boundary conditions instead of the prescribed open boundary conditions. In the absence of any perturbation, the jet is stable. The addition of the seamounts bottom topography induces a perturbation and allows us to quantify the growth rates of the instability for each configuration. Figure 14 displays a snapshot of the u component of the velocity after 38 days for the same topography as F1–F4 (Fig. 11), respectively. The growth rate of the instability is significantly faster (on the order of 50%) in the experiments with wide seamounts (Figs. 14a,c) than in the experiments with narrow seamounts (Figs. 14b,d), a

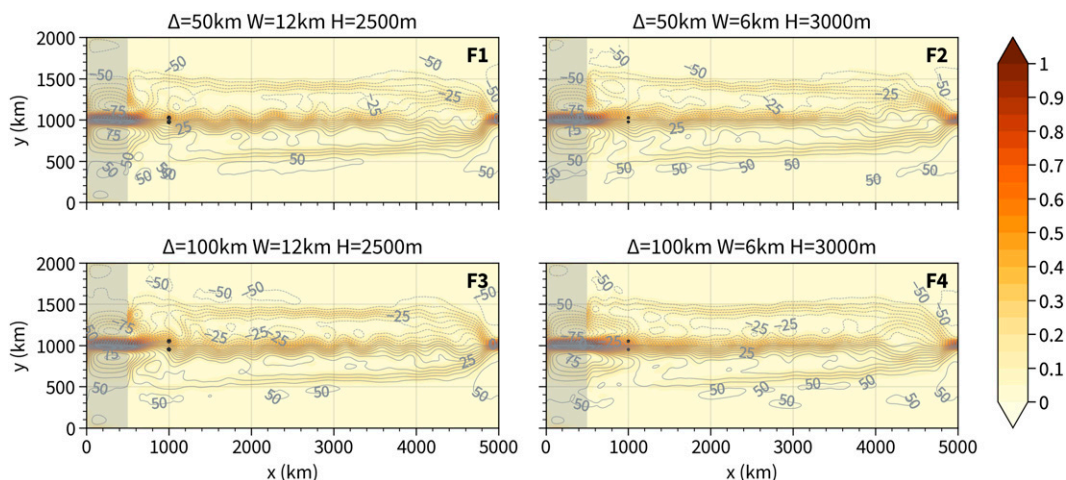


FIG. 12. Two-year mean SSH (cm) for the fine-resolution experiments F1–F4 (Table 3) superimposed on the upper-layer velocity (m s^{-1}). The two seamounts (dark-brown contours) are positioned 500 km downstream of the prescribed open boundary relaxation area (shaded in gray).

result consistent with the linear stability analysis performed in the previous section.

4. Summary and conclusions

Bathymetry affects time-dependent motion throughout the water column and the series of experiments presented in this paper highlight the importance of properly resolving the NESC when modeling the Gulf Stream. The NESC has a strong impact on the Gulf Stream pathway and variability, as demonstrated by comparison experiments with and without the NESC. In the absence of the NESC, the Gulf Stream stays coherent much farther east than in the experiment with the NESC; that is, the NESC destabilizes the Gulf Stream. When the NESC is not properly resolved by the models' grid, the

impact on the Gulf Stream's pathway and variability is surprisingly large. The differences between the $1/12^\circ$ (~ 6 km) and $1/50^\circ$ (~ 1.5 km) bathymetries are not very big (Fig. 1) but are sufficient to significantly impact the Gulf Stream pathway and variability. Idealized channel experiments were used to 1) reconcile the results obtained with the high-resolution North and equatorial HYCOM Atlantic configurations and earlier coarse-resolution NESC sensitivity experiments by Adamec (1988) and Ezer (1994) and 2) quantify how much of an impact narrower and taller seamounts have on a surface jet when compared with wider and shorter seamounts. The result is intuitive, with narrower and taller seamounts creating a smaller horizontal extent of unstable flows.

Chassignet and Xu (2017) argued that the next threshold for a significant improvement in western boundary currents

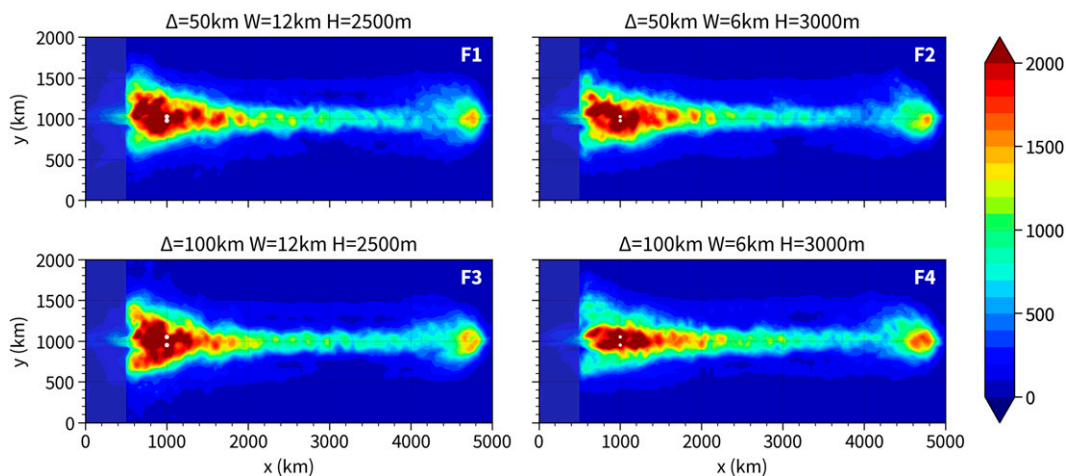


FIG. 13. Two-year mean upper-layer eddy kinetic energy ($\text{cm}^2 \text{s}^{-2}$) for the fine-resolution experiments F1–F4 (Table 3). The white dots at 1000 km mark the location of the seamounts.

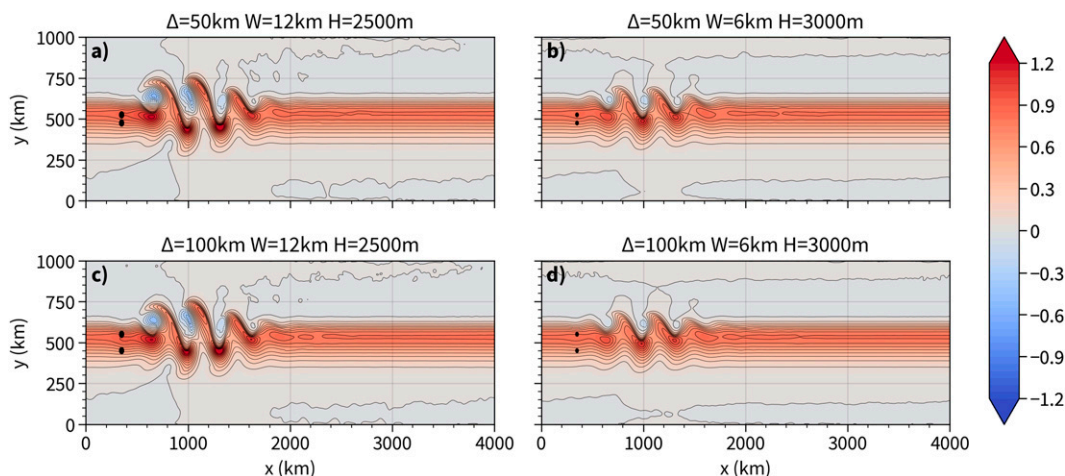


FIG. 14. Snapshot of the u component of the velocity (m s^{-1}) after 38 days of the cyclic experiments with the same topography as in F1–F4 (Table 3).

representation is an increase in the horizontal resolution from the eddying $1/10^\circ$ to submesoscale enabled $1/50^\circ$ grid spacing. However, resolving the submesoscale is not the only gain from using kilometeric-resolution models; there is also the benefit of a better representation of the topography as previously demonstrated by Ezer (2016) and Schoonover et al. (2016). Here, we demonstrated the impact of fine topography on the Gulf Stream, but better resolved bathymetry will also have an impact elsewhere in the model domain, for example on transports through straits and on the representation of overflows. Submesoscale-resolving ocean models are computationally very expensive such as the ones discussed here, and most state-of-the-art global and basin-scale simulations can only be run for short periods of time. It will be some time before they become more routine and can be used operationally and in climate models. Introducing a correction term to account for fine-scale topography may be a way to improve flow–topographic interaction under coarse model resolution (Debreu et al. 2022). In addition, models with kilometer-scale resolution generate a large number of outputs, to the point that it becomes challenging to extract useful information from the stored archives. To address this dissemination and analysis challenge of these large model outputs, Uchida et al. (2022) recently showcased a cloud-based analysis framework and showed that a cloud-based analysis framework minimizes the cost of duplicating and storing ghost copies of data and allows for seamless sharing of model outputs among collaborators and systematically analyzing them in a self-consistent manner. Namely, the cloud-based framework allows users to apply the same analysis methods across different datasets, which can then highlight the differences resulting from the model numerics themselves. Given the impact of minor changes in bathymetry on oceanic jets, as shown in this study, we agree with Uchida et al. (2022) that an emphasis on data analysis strategies is crucial for improving the realism of the models themselves and is essential if one is to identify the impact of the numerical and/or configuration choices

(such as the representation of the bathymetry) made by the various modeling groups.

Acknowledgments. Authors Chassignet, Xu, and Bozec were supported by the Office of Naval Research (Grants N00014-19-1-2717 and N00014-20-1-2769) and the NSF Physical Oceanography Program (Award 2038449). Author Uchida acknowledges support from NSF Grant OCE-2123632. This work is a contribution to SWOT through the NASA Grant NNX16AH79G. The numerical simulations were performed on supercomputers at the Navy DoD Supercomputing Resource Center, Stennis Space Center, Mississippi, using computer time provided by the U.S. DoD High Performance Computing Modernization Program.

Data availability statement. All model outputs are available upon request.

REFERENCES

- Abernathey, R., and Coauthors, 2023: XGCM: General circulation model postprocessing with xarray. Zenodo, accessed 27 December 2022, <https://doi.org/10.5281/zenodo.3634752>.
- Adamec, D., 1988: Numerical simulations of the effects of sea-mounts and vertical resolution on strong ocean flows. *J. Phys. Oceanogr.*, **18**, 258–269, [https://doi.org/10.1175/1520-0485\(1988\)018<0258:NSOTEO>2.0.CO;2](https://doi.org/10.1175/1520-0485(1988)018<0258:NSOTEO>2.0.CO;2).
- Andres, M., 2016: On the recent destabilization of the Gulf Stream path downstream of Cape Hatteras. *Geophys. Res. Lett.*, **43**, 9836–9842, <https://doi.org/10.1002/2016GL069966>.
- Auer, S. J., 1987: Five-year climatological survey of the Gulf Stream system and its associated rings. *J. Geophys. Res.*, **92**, 11 709–11 726, <https://doi.org/10.1029/JC092iC11p11709>.
- Barthel, A., A. M. Hogg, S. Waterman, and S. Keating, 2017: Jet–topography interactions affect energy pathways to the deep Southern Ocean. *J. Phys. Oceanogr.*, **47**, 1799–1816, <https://doi.org/10.1175/JPO-D-16-0220.1>.

- Bleck, R., 2002: An oceanic general circulation model framed in hybrid isopycnic-Cartesian coordinates. *Ocean Modell.*, **4**, 55–88, [https://doi.org/10.1016/S1463-5003\(01\)00012-9](https://doi.org/10.1016/S1463-5003(01)00012-9).
- Carnes, M. R., 2009: Description and evaluation of GDEM-V3.0. NRL Memo. Rep. NRL/MR/7330-09-9165, 24 pp., <https://www.7320.nrlssc.navy.mil/pubs/2009/carnes-2009.pdf>.
- Chassignet, E. P., and X. Xu, 2017: Impact of horizontal resolution ($1/12^\circ$ to $1/50^\circ$) on Gulf Stream separation, penetration, and variability. *J. Phys. Oceanogr.*, **47**, 1999–2021, <https://doi.org/10.1175/JPO-D-17-0031.1>.
- , and —, 2021: On the importance of high-resolution in large scale ocean models. *Adv. Atmos. Sci.*, **38**, 1621–1634, <https://doi.org/10.1007/s00376-021-0385-7>.
- , L. T. Smith, G. R. Halliwell, and R. Bleck, 2003: North Atlantic simulations with the Hybrid Coordinate Ocean Model (HYCOM): Impact of the vertical coordinate choice, reference pressure, and thermobaricity. *J. Phys. Oceanogr.*, **33**, 2504–2526, [https://doi.org/10.1175/1520-0485\(2003\)033<2504:NASWTH>2.0.CO;2](https://doi.org/10.1175/1520-0485(2003)033<2504:NASWTH>2.0.CO;2).
- , and Coauthors, 2006: Generalized vertical coordinates for eddy-resolving global and coastal ocean forecasts. *Oceanography*, **19**, 118–129, <https://doi.org/10.5670/oceanog.2006.95>.
- Cornillon, P., 1986: The effect of the New England Seamounts on Gulf Stream meandering as observed from satellite IR imagery. *J. Phys. Oceanogr.*, **16**, 386–389, [https://doi.org/10.1175/1520-0485\(1986\)016<0386:TEOTNE>2.0.CO;2](https://doi.org/10.1175/1520-0485(1986)016<0386:TEOTNE>2.0.CO;2).
- Debreu, L., N. K.-R. Kevlahan, and P. Marchesiello, 2022: Improved Gulf Stream separation through Brinkman penalization. *Ocean Modell.*, **179**, 102121, <https://doi.org/10.1016/j.ocemod.2022.102121>.
- Ezer, T., 1994: On the interaction between the Gulf Stream and the New England seamount chain. *J. Phys. Oceanogr.*, **24**, 191–204, [https://doi.org/10.1175/1520-0485\(1994\)024<0191:OTIBTG>2.0.CO;2](https://doi.org/10.1175/1520-0485(1994)024<0191:OTIBTG>2.0.CO;2).
- , 2016: Revisiting the problem of the Gulf Stream separation: On the representation of topography in ocean models with different types of vertical grids. *Ocean Modell.*, **104**, 15–27, <https://doi.org/10.1016/j.ocemod.2016.05.008>.
- Fuglister, F. C., 1963: Gulf Stream '60. *Prog. Oceanogr.*, **1**, 265–373, [https://doi.org/10.1016/0079-6611\(63\)90007-7](https://doi.org/10.1016/0079-6611(63)90007-7).
- Gangopadhyay, A., A. H. Chaudhuri, and A. H. Taylor, 2016: On the nature of temporal variability of the Gulf Stream path from 75° to 55° W. *Earth Interact.*, **20**, <https://doi.org/10.1175/EI-D-15-0025.1>.
- Hansen, D. V., 1970: Gulf stream meanders between Cape Hatteras and the Grand Banks. *Deep-Sea Res. Oceanogr. Abstr.*, **17**, 495–511, [https://doi.org/10.1016/0011-7471\(70\)90064-1](https://doi.org/10.1016/0011-7471(70)90064-1).
- Holland, W. R., and A. D. Hirschman, 1972: A numerical calculation of the circulation in the North Atlantic Ocean. *J. Phys. Oceanogr.*, **2**, 336–354, [https://doi.org/10.1175/1520-0485\(1972\)002<0336:ANCOTC>2.0.CO;2](https://doi.org/10.1175/1520-0485(1972)002<0336:ANCOTC>2.0.CO;2).
- Holton, J. R., and G. J. Hakim, 2013: *An Introduction to Dynamic Meteorology*. 5th ed. Academic Press, 552 pp., <https://doi.org/10.1016/C2009-0-63394-8>.
- Houghton, R. L., J. R. Heirtzler, R. D. Ballard, and P. T. Taylor, 1977: Submersible observations of the New England seamounts. *Naturwissenschaften*, **64**, 348–355, <https://doi.org/10.1007/BF00368733>.
- Huppert, H. E., and K. Bryan, 1976: Topographically generated eddies. *Deep-Sea Res. Oceanogr. Abstr.*, **23**, 655–679, [https://doi.org/10.1016/S0011-7471\(76\)80013-7](https://doi.org/10.1016/S0011-7471(76)80013-7).
- Hurlburt, H. E., and P. J. Hogan, 2000: Impact of $1/8^\circ$ to $1/64^\circ$ resolution on Gulf Stream model–data comparisons in basin-scale subtropical Atlantic Ocean models. *Dyn. Atmos. Oceans*, **32**, 283–329, [https://doi.org/10.1016/S0377-0265\(00\)00050-6](https://doi.org/10.1016/S0377-0265(00)00050-6).
- Jamet, Q., B. Deremble, N. Wienders, T. Uchida, and W. K. Dewar, 2021: On wind-driven energetics of subtropical gyres. *J. Adv. Model. Earth Syst.*, **13**, e2020MS002329, <https://doi.org/10.1029/2020MS002329>.
- Kämpf, J., 2005: Cyclogenesis in the deep ocean beneath western boundary currents: A process-oriented numerical study. *J. Geophys. Res.*, **110**, C03001, <https://doi.org/10.1029/2003JC002206>.
- LaCasce, J. H., and S. Groeskamp, 2020: Baroclinic modes over rough bathymetry and the surface deformation radius. *J. Phys. Oceanogr.*, **50**, 2835–2847, <https://doi.org/10.1175/JPO-D-20-0055.1>.
- Li, Y., T. McDougall, S. Keating, C. de Lavergne, and G. Madec, 2019: Horizontal residual mean: Addressing the limited spatial resolution of ocean models. *J. Phys. Oceanogr.*, **49**, 2741–2759, <https://doi.org/10.1175/JPO-D-19-0092.1>.
- McDougall, T., and P. Baker, 2011: Getting started with TEOS-10 and the Gibbs Seawater (GSW) Oceanographic Toolbox. SCOR/IASPO WG127, 28 pp., https://www.teos-10.org/pubs/gsw/v3_04/pdf/Getting_Started.pdf.
- Meinen, C. S., and D. S. Luther, 2016: Structure, transport and vertical coherence of the Gulf Stream from the Straits of Florida to the Southeast Newfoundland Ridge. *Deep-Sea Res. I*, **111**, 16–17, <https://doi.org/10.1016/j.dsr.2016.02.002>.
- Mellor, G. L., T. Ezer, and L.-Y. Oey, 1994: The pressure gradient conundrum of sigma coordinate ocean models. *J. Atmos. Oceanic Technol.*, **11**, 1126–1134, [https://doi.org/10.1175/1520-0426\(1994\)011<1126:TPGCOS>2.0.CO;2](https://doi.org/10.1175/1520-0426(1994)011<1126:TPGCOS>2.0.CO;2).
- Mertz, G., and D. G. Wright, 1992: Interpretations of the JEBAR term. *J. Phys. Oceanogr.*, **22**, 301–305, [https://doi.org/10.1175/1520-0485\(1992\)022<0301:IOTJT>2.0.CO;2](https://doi.org/10.1175/1520-0485(1992)022<0301:IOTJT>2.0.CO;2).
- Mulet, S., and Coauthors, 2021: The new CNES-CLS18 global mean dynamic topography. *Ocean Sci.*, **17**, 789–808, <https://doi.org/10.5194/os-17-789-2021>.
- Richardson, P. L., 1981: Gulf Stream trajectories measured with free-drifting buoys. *J. Phys. Oceanogr.*, **11**, 999–1010, [https://doi.org/10.1175/1520-0485\(1981\)011<0999:GSTMWF>2.0.CO;2](https://doi.org/10.1175/1520-0485(1981)011<0999:GSTMWF>2.0.CO;2).
- Savidge, D. K., and J. M. Bane Jr., 1999: Cyclogenesis in the deep ocean beneath the Gulf Stream: 2. Dynamics. *J. Geophys. Res.*, **104**, 18 127–18 140, <https://doi.org/10.1029/1999JC900131>.
- Schoonover, J., and Coauthors, 2016: North Atlantic barotropic vorticity balances in numerical models. *J. Phys. Oceanogr.*, **46**, 289–303, <https://doi.org/10.1175/JPO-D-15-0133.1>.
- Schubert, R., A. Biastoch, M. F. Cronin, and R. J. Greatbatch, 2018: Instability-driven benthic storms below the separated Gulf Stream and the North Atlantic Current in a high-resolution ocean model. *J. Phys. Oceanogr.*, **48**, 2283–2303, <https://doi.org/10.1175/JPO-D-17-0261.1>.
- Seidov, D., A. Mishonov, J. Reagan, and R. Parsons, 2019: Resilience of the Gulf Stream path on decadal and longer timescales. *Sci. Rep.*, **9**, 11549, <https://doi.org/10.1038/s41598-019-48011-9>.
- Silver, A., A. Gangopadhyay, G. Gawarkiewicz, E. N. S. Silva, and J. Clark, 2021: Interannual and seasonal asymmetries in Gulf Stream Ring Formations from 1980 to 2019. *Sci. Rep.*, **11**, 2207, <https://doi.org/10.1038/s41598-021-81827-y>.
- Smith, K. S., 2007: The geography of linear baroclinic instability in Earth's oceans. *J. Mar. Res.*, **65**, 655–683.
- Smith, W. H. F., and D. T. Sandwell, 1997: Global sea floor topography from satellite altimetry and ship depth soundings. *Science*, **277**, 1956–1962, <https://doi.org/10.1126/science.277.5334.1956>.

- Teague, W. J., and Z. R. Hallock, 1990: Gulf Stream path analysis near the New England Seamounts. *J. Geophys. Res.*, **95**, 1647–1662, <https://doi.org/10.1029/JC095iC02p01647>.
- , M. J. Carron, and P. J. Hogan, 1990: A comparison between the generalized digital environmental model and Levitus climatologies. *J. Geophys. Res.*, **95**, 7167–7183, <https://doi.org/10.1029/JC095iC05p07167>.
- Thompson, J. D., and W. J. Schmitz Jr., 1989: A limited-area model of the Gulf Stream: Design, initial experiments, and model-data intercomparison. *J. Phys. Oceanogr.*, **19**, 791–814, [https://doi.org/10.1175/1520-0485\(1989\)019<0791:ALAMOT>2.0.CO;2](https://doi.org/10.1175/1520-0485(1989)019<0791:ALAMOT>2.0.CO;2).
- Uchida, T., R. Abernathy, and S. Smith, 2017: Seasonality of eddy kinetic energy in an eddy permitting global climate model. *Ocean Modell.*, **118**, 41–58, <https://doi.org/10.1016/j.oceanmod.2017.08.006>.
- , and Coauthors, 2022: Cloud-based framework for inter-comparing submesoscale-permitting realistic ocean models. *Geosci. Model Dev.*, **15**, 5829–5856, <https://doi.org/10.5194/gmd-15-5829-2022>.
- Uppala, S. M., and Coauthors, 2005: The ERA-40 re-analysis. *Quart. J. Roy. Meteor. Soc.*, **131**, 2961–3012, <https://doi.org/10.1256/qj.04.176>.
- Vallis, G. K., 2017: *Atmospheric and Oceanic Fluid Dynamics*. Cambridge University Press, 205 pp.
- Vastano, A. C., and B. A. Warren, 1976: Perturbations to the Gulf Stream by Atlantis II Seamount. *Deep-Sea Res. Oceanogr. Abstr.*, **23**, 681–694, [https://doi.org/10.1016/S0011-7471\(76\)80014-9](https://doi.org/10.1016/S0011-7471(76)80014-9).
- Verron, J., C. Le Provost, and W. R. Holland, 1987: On the effects of a midocean ridge on the general circulation: Numerical simulations with an eddy-resolved ocean model. *J. Phys. Oceanogr.*, **17**, 301–312, [https://doi.org/10.1175/1520-0485\(1987\)017<0301:OTEOAM>2.0.CO;2](https://doi.org/10.1175/1520-0485(1987)017<0301:OTEOAM>2.0.CO;2).
- Xu, X., E. P. Chassignet, A. J. Wallcraft, B. K. Arbic, M. C. Buijsman, and M. Solano, 2022: On the spatial variability of the sea surface height wavenumber spectra in the Atlantic Ocean. *J. Geophys. Res. Oceans*, **127**, e2022JC018769, <https://doi.org/10.1029/1272022JC018769>.
- Yankovsky, E., L. Zanna, and K. S. Smith, 2022: Influences of mesoscale ocean eddies on flow vertical structure in a resolution-based model hierarchy. *J. Adv. Model. Earth Syst.*, **14**, e2022MS003203, <https://doi.org/10.1029/2022MS003203>.
- Young, W. R., 2012: An exact thickness-weighted average formulation of the Boussinesq equations. *J. Phys. Oceanogr.*, **42**, 692–707, <https://doi.org/10.1175/JPO-D-11-0102.1>.